

L. CIURCĂ¹, B. PRICOP¹, M. AGOP¹, L.-G. BUJOREANU^{1*}

ON BENDING CREEP BEHAVIOUR OF A POWDER METALLURGY FeMnSiCrNi SHAPE MEMORY ALLOY

FeMnSiCrNi alloys represent a promising class of FeMnSi-based shape memory alloys (SMAs) characterized by excellent characteristics of formability and corrosion resistance. The present paper is focused on a 68Fe-18Mn-3Si-7Cr-4Ni (mass. %) SMA, produced by powder metallurgy routine, which was tested to creep, using a dual cantilever specimen holder, and analyzed by means of the dedicated software of a dynamic mechanical analyzer. The specimens were tested at five temperatures by applying, at each of them, four bending force values, during 2000 s. The variation of bending creep deflection with time, temperature and force was discussed both from the point of instant value and 1000 s-value. These results enabled plotting a space diagram of stabilized creep rate variation with both applied force and test temperature. In such context, a theoretical model in a multifractal paradigm of motion was built, considering that FeMnSiCrNi shape memory alloy can be assimilated, both structurally and functionally, with a multifractal object. Finally, this model was validated by means of experimental data.

Keywords: FeMnSiCrNi shape memory alloy; bending creep; creep rate; multifractal model

1. Introduction

FeMnSiCrNi shape memory alloys (SMAs) have been developed since 1990, after Otsuka et al. added Cr, to FeMnSi system, in order to enhance corrosion resistance [1] and Moriya et al. put in Ni to suppress the formation of σ phase which reduces workability [2]. Besides corrosion resistance, FeMnSiCrNi SMAs have been characterized by relatively high recovery deformations. Thus, Wen et al. reported a recovery strain of 7.6% in Fe-20.2Mn-5.6Si-8.9Cr-5.0Ni steel (weight %) annealed for 12.5 h at 1,373 K and subjected to four training cycles in bending [3]. Similarly, Peng et al. obtained a recovery strain of 7.7% in cast Fe-19Mn-5.5Si-9Cr-4.5Ni alloy with the coarse austenitic grains of 652 μm [4].

These features enhanced the development of pipe couplings made from Fe-15Mn-5Si-9Cr-5Ni (wt. %) SMA and even of 2-tons earthquake-resistant dampers made of Fe-15Mn-4Si-10Cr-8Ni (mass. %) alloy for the seismic protection of “JP Tower Nagoya” [5].

On the other hand, Pricop et al. argued that powder metallurgy (PM) routine could be an useful alternative for FeMnSiCrNi SMA processing [6]. From Fe-14Mn-6Si-9Cr-5Ni SMA, containing mechanically alloyed powder particles, two types of potential applications could be manufactured: (i) actuator type,

based on storage modulus-increase on heating that exceeded 1 GPa [7] and (ii) couplings, for the safe connection of pipes that vibrate during transportation of turbulent fluids [8]. In this sense, the present authors tested an Fe-18Mn-3Si-7Cr-4Ni (mass. %) SMA produced from commercial powders with zinc stearate binder, and determined second order polynomials, that modelled the saturation tendencies of total and permanent strains during 100 tensile loading-unloading cycles performed up to 600 MPa [9].

Common models used to describe the creep phenomena in material science, have been based either on a combination of basic theories, derived especially from physics or on computer simulations [10-15]. In such a context, their description has implied both computational simulations based on specific algorithms [13-15], as well as developments on standard theories. With respect to models developed on standard theories, the following classes can be distinguished:

- i) A class of models developed on spaces with integer dimension – *i.e.* differentiable models (for example, developments based on Generalized Hooke Laws etc.) [10-12].
- ii) Another class of models developed on spaces with non-integer dimensions, which are explicitly written through fractional derivatives [14,15] – *i.e.* non – differentiable models, with examples including the fractal models.

¹ GHEORGHE ASACHI TECHNICAL UNIVERSITY OF IAȘI, FACULTY OF MATERIALS SCIENCE AND ENGINEERING BLVD. DIMITRIE MANGERON 61A. 700050 IAȘI, ROMANIA

* Corresponding author: lgbujor@tuiasi.ro



iii) Expanding the previous class of models, new developments have been made, based on Scale Relativity Theory, either in the monofractal dynamics as in the case of Nottale [16], or in the multifractal dynamics as in the case of the Multifractal Theory of Motion [17,18].

Both in the context of Scale Relativity Theory in the sense of Nottale [16], as well as in the one of Multifractal Theory of Motion [17,18], the fundamental hypothesis have been the following: supposing that any type of matter (for example alloys, biocomposites etc.) was assimilated both structurally and functionally to a multifractal object, said dynamics can be described through motions of any matter's structural units, dependent on the chosen scale resolution, on continuous and non – differentiable curves (multifractal curves).

Such a hypothesis may be illustrated by considering the following scenario: between two successive interactions of the structural units belonging to any matter, the trajectory of the matter's structural unit is a straight line that became non-differentiable in the impact point. Considering that all interaction points formed an uncountable set of points, it results that the trajectories of the matter's structural units became continuous and non-differentiable (*i.e.* fractal curves). Clearly, the reality has been much more complicated, taking into account both the diversity of the structural units which compose any matter and the various interactions between them in the form of double interactions etc. Extrapolating the previous reasoning for any type of matter, including the FeMnSiCrNi SMA, it results that it can be assimilated to a multifractal.

All these considerations implied that, in the description of the FeMnSiCrNi SMA dynamics, instead of “working” with a single variable (regardless of its nature, *i.e.*, velocity, density, etc.) described by a strict non – differentiable function, it has been possible to “work” only with approximations of this mathematical function, obtained by averaging them on different scale resolutions. As a consequence, any variable purposed to describe the FeMnSiCrNi SMA dynamics will perform as the limit of a family of mathematical functions, this being non – differentiable for null scale resolutions and differentiable otherwise [16-18]. To put it differently, from a mathematical point of view, these variables could be explained through multifractal functions, *i.e.* functions dependent not only on spatial and temporal coordinates, but also on the scale resolution.

Since for a large temporal scale resolution with respect to the inverse of the highest Lyapunov exponent [19,20], the deterministic trajectories of any structural unit belonging to the FeMnSiCrNi SMA, can be replaced by a collection of potential (“virtual”) trajectories. Thus, the concept of definite trajectory can be substituted by the one of probability density.

With all of the above considerations taken into account, the multifractality expressed through stochasticity, in the description of the dynamics of any FeMnSiCrNi SMA, became operational in the multifractal paradigm through the Multifractal Theory of Motion. It was noticed that various applications of this model have been described in [21-33].

In this context, the present study was directed to the experimental study of creep phenomena occurring in a PM Fe-18Mn-3Si-7Cr-4Ni (mass. %) SMA subjected to three-point-bending and to the modelling of its behavior. A mathematical model was created considering the FeMnSiCrNi SMA as a multifractal object, and analyzing its dynamics in the framework of Scale Relativity Theory, using various operational procedures (Riccati-type gauges and invariance groups). Finally, the theoretical model was validated by means of the experimental data.

2. Experimental procedure

Rectangular ($1 \times 4 \times 50$ mm) specimens were cut by wire spark erosion from an Fe-18Mn-3Si-7Cr-4Ni (mass. %) SMA which was pressed, sintered, homogenized and hot-rolled as previously pointed out [9].

The specimens were investigated by dynamic mechanical analysis (DMA), comprising temperature scans (TS) and creep tests (CT), performed by means of a NETZSCH DMA 242 Artemis device, using a dual cantilever specimen holder and PROTEUS software both for thermal analysis and for creep and relaxation.

For temperature scans, the specimens were heated from room temperature to 400°C with a heating rate of 5°C/min and a frequency of 1 Hz. DMA-TS diagrams present the variation, with temperature, of both storage modulus (E') and the ratio of loss modulus (E'') and storage modulus designated as internal friction, $\tan d = E''/E'$. One representative example is shown in Fig. 1.

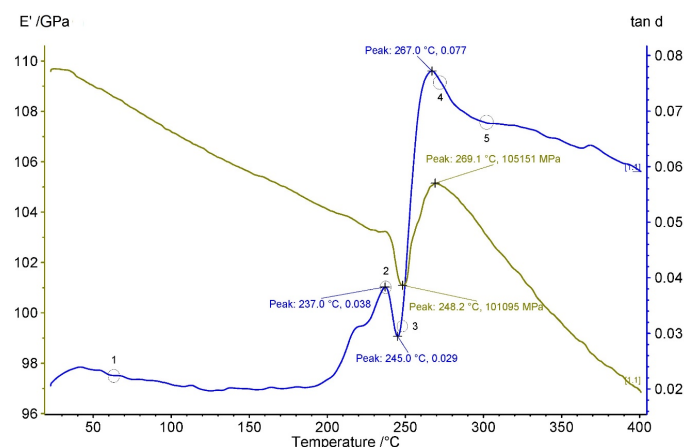


Fig. 1. DMA temperature scan thermogram illustrating the variation of storage modulus (E') and internal friction ($\tan d$) with temperature, during heating of a PM Fe-18Mn-3Si-7Cr-4Ni (mass. %) SMA

As previously pointed out, there are two $\tan d$ maxima. The low-intensity maximum, located at lower temperatures corresponds to antiferromagnetic \Rightarrow paramagnetic transition, overlapped with the reversion of α' -body centered cubic (*bcc*) martensite to γ -face centered cubic (*fcc*) austenite and the higher intensity one to ε -hexagonal close packed (*hcp*) \Rightarrow γ (*fcc*) reverse

martensitic transformation [6,8]. Based on these considerations, five temperatures were selected for creep tests: 60°C, 233°C, 248°C, 270°C and 300°C. These temperatures correspond to five different states, numbered from 1 to 5 in Fig. 1. *State 1* – fully antiferromagnetic martensite, at 60°C; *state 2* – half antiferromagnetic martensite-half paramagnetic martensite, corresponding to temperature $A_{N(\tan\delta)}^{50}$, $\tan\delta$ peak at 233°C; *state 3* – full paramagnetic martensite, E' minimum at 248°C; *state 4* – half paramagnetic martensite-half austenite, corresponding to temperature $A_{\varepsilon(E')}^{50}$ and *state 5* – fully austenitic.

During experimental creep investigations, the approach used by Leinenbach et al. for the study of low-temperature creep and stress relaxation behavior of an Fe-17Mn-5Si-10Cr-4Ni-1(V,C) (mass.%) was applied [34].

The experiments were performed by using the creep end relaxation variant of PROTEUS software. Four specimens were fastened in the dual cantilever specimen holder that fixes the specimen both at its ends and its middle. On turn, each specimen was bent by four different applied forces, 1 N, 3 N, 6 N and 9 N, respectively. After 2000 s of deformation, at a given force and temperature, the device's pushrod unloads the specimen and brings it back to zero deflection. Then, the specimen is heated to the next temperature from the above listed values and the same force is applied for 2000 s. The same procedure applies from 60°C to 300°C, with a given force. Then, next specimen is used

and the procedure is repeated for the next bending force. Force values were adopted below 12 N, which represents the blocking force of the analyzer, due to self-protection reasons. In each case, the DMA device measured the variation of bending deflection with time and, based on specimens' dimensions, PROTEUS software determined the rest of the parameters.

3. Experimental results and discussion

3.1. Creep tests

The first set of experimental results comprises the variation of bending deflection during the application of the four experimental forces, for a period of 2000 s, at each of the five above-mentioned temperatures. The results are summarized in Fig. 2.

Obviously, each diagram displays a two-stage creep behavior: (i) initial/primary creep, with sudden high rate deformation and (ii) stabilized/secondary creep, which developed at almost constant reduced rate, up to the end of testing time. In each case, according to [34] the creep strain reached after 1000 s creep time was listed μm , under the form $d_{1000}^{T_i}$, where T_i are the values of the five above-mentioned test temperatures.

It is obvious that creep deformation increased both with applied force and test temperature. At low applied forces, 1 and

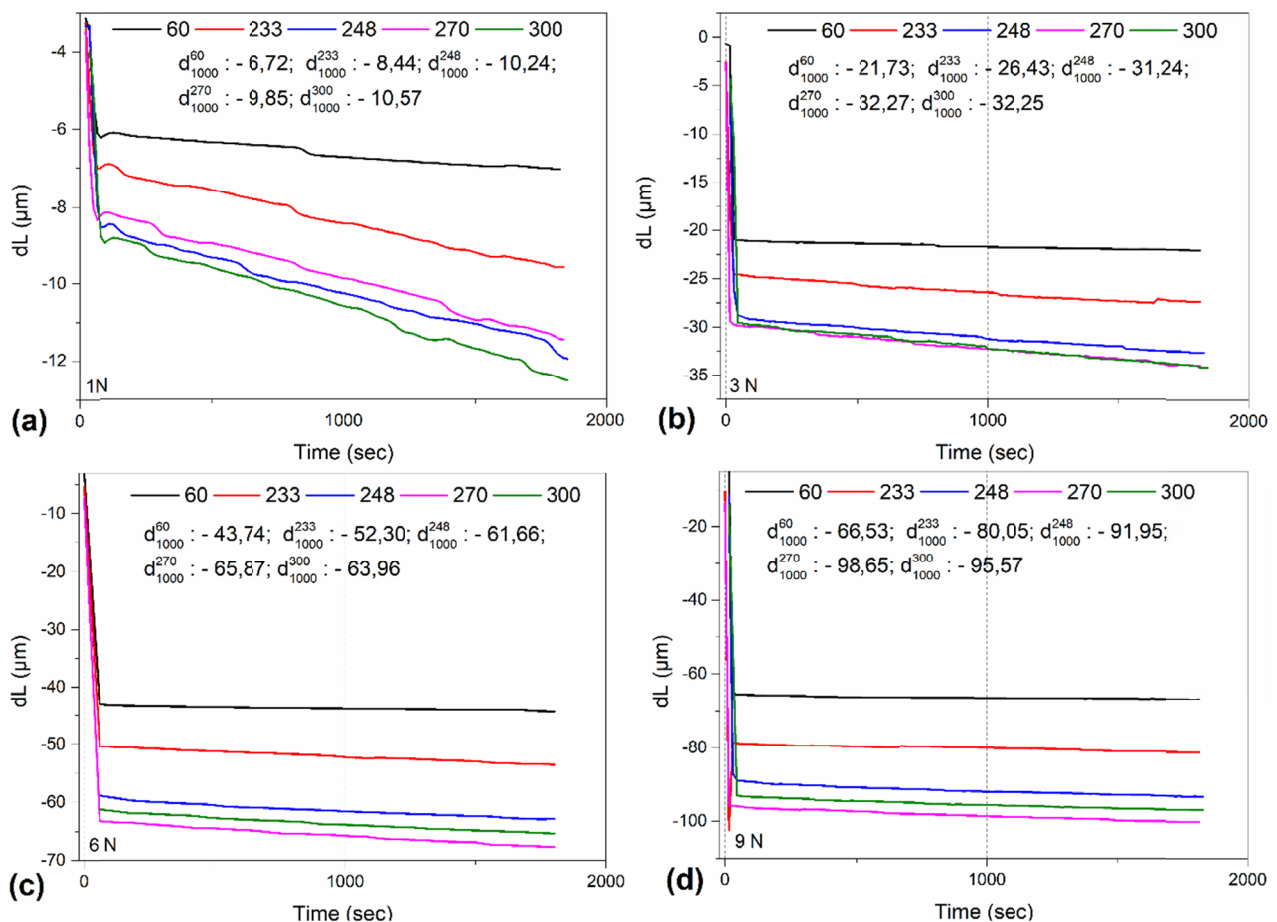


Fig. 2. Variation of bending deflection in time, at five testing temperatures, under the effect of different bending forces: (a) 1 N; (b) 3 N; (c) 6 N and (d) 9 N. The values listed as $d_{1000}^{T_i}$ correspond to the creep strain reached after 1000 s creep time (μm) at each respective test temperature, T_i

3 N, creep deformation increased almost monotonically with test temperature, in Figs 2(a) (excepting for the values obtained at 248°C, which are about 0.5 μm larger than those obtained at 270°C) and 2(b). At higher forces, 6 and 9 N, Figs 2(c) and (d) show that creep deformations at 270°C, in half paramagnetic martensitic-half austenitic state, were superior with about 3 μm to those measured at 300°C, in fully austenitic state. This could be an effect of cumulating the increase in high temperature atomic vibration amplitudes with the destabilization of paramagnetic martensite. In each of the four diagrams from Fig. 2, bending deflection markedly increased while passing from fully antiferromagnetic martensite (at 60°C), to half antiferromagnetic -half paramagnetic martensite (at 233°C) and finally to fully paramagnetic martensite (at 248°C). It is obvious that the increases in bending deflection, between the three states, are almost equal. On the other hand, bending deformation seems to be less sensitive to further temperature increase from fully paramagnetic martensite (at 248°C), to half paramagnetic martensite-half austenite (at 270°C) and finally to fully austenitic state (at 300°C).

Maximum creep deformation reached 100 μm , after applying the 9 N force for 2000 s at 270°C.

Both initial and stabilized creep regions of the curves displayed in Fig. 2 were fitted with first degree functions. The slopes of these linear fits represent creep rates and are plotted in Fig. 3.

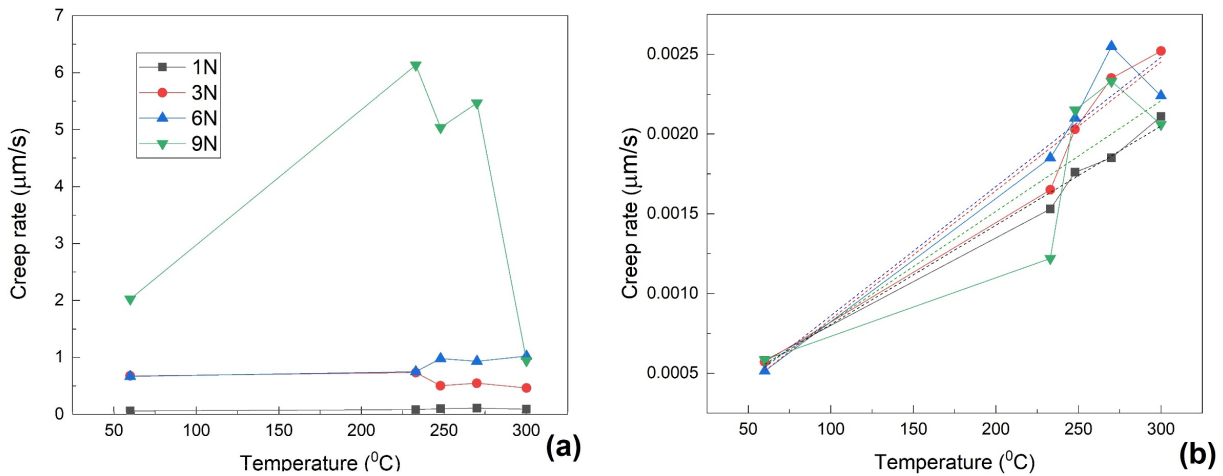


Fig. 3. Creep rate variation with temperature, under four different applied forces: (a) during initial creep; (b) during stabilized creep, with linear fits

TABLE 1

Results of linear fits of the variation of secondary creep rate (y , in $\mu\text{m/s}$) with temperature (x , in $^{\circ}\text{C}$), according to Fig. 3(b)

Applied bending force	1 N	3 N	6 N	9 N
Equation	$y = a + b * x$			
Intercept, a ($\mu\text{m/s}$)	1.8276×10^{-4} $\pm 9.23469 \times 10^{-5}$	3.09084×10^{-5} $\pm 2.25434 \times 10^{-4}$	5.00388×10^{-5} $\pm 2.96418 \times 10^{-4}$	1.28809×10^{-4} $\pm 5.14306 \times 10^{-4}$
Slope, b [$\mu\text{m}/(\text{s} \times ^{\circ}\text{C})$]	6.22471×10^{-6} $\pm 3.88649 \times 10^{-7}$	8.07077×10^{-6} $\pm 9.48755 \times 10^{-7}$	8.10344×10^{-6} $\pm 1.2475 \times 10^{-6}$	6.93074×10^{-6} $\pm 2.16449 \times 10^{-6}$
Residual Sum of Squares	1.60543×10^{-8}	9.56722×10^{-8}	1.65408×10^{-7}	4.97955×10^{-7}
Pearson's r	0.9942	0.97989	0.96624	0.87956
R-Square (COD)	0.98844	0.96019	0.93362	0.77363
Adj. R-Square	0.98459	0.94692	0.91149	0.69818

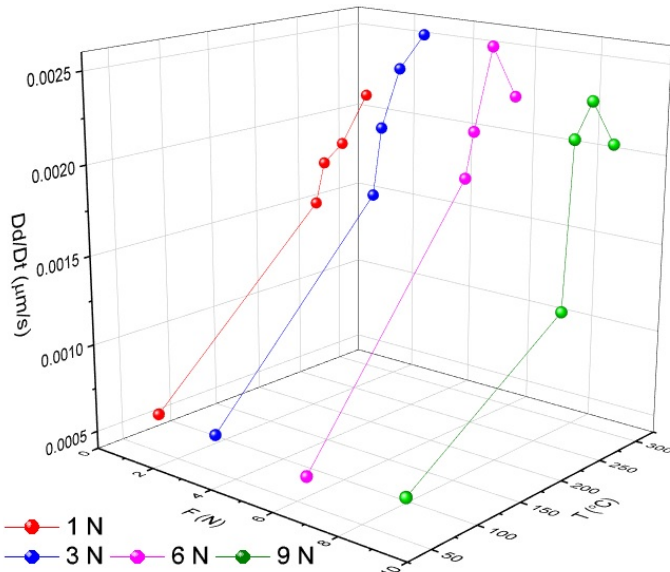


Fig. 4. Space diagram illustrating the effects of applied force and testing temperature on deflection rate variation during stabilized creep

3.2. Mathematical model

3.2.1. Stresses – strains correlations of multifractal type

According with the Multifractal Theory of Motion in the form of multifractal hydrodynamic model [17,18], the specific multifractal potential Q ,

$$Q = -2\lambda^2 (dt) \left[\frac{4}{f(x)} \right]^{-2} \frac{\partial l \partial_l \sqrt{\rho}}{\sqrt{\rho}} \tag{1}$$

induces the multifractal stress tensor $\hat{\sigma}_{il}$,

$$\hat{\sigma}_{il} = -2\lambda^2 (dt) \left[\frac{4}{f(\alpha)} \right]^{-2} \rho \partial_i \partial_l (\ln \rho) \tag{2}$$

the divergence of which is equal to the multifractal force density associated with Q :

$$\partial^i \hat{\sigma}_{il} + \rho \partial_i Q = 0 \tag{3}$$

where

$$\partial_l = \frac{\partial}{\partial X^l}, f(\alpha) = f[\alpha(D_F)] \tag{4}$$

In equations (1)-(3) ρ is the density of states, t is the non-multifractal time with the role of affine parameter of the motion curves, X^l are the multifractal spatial coordinates, dt is the scale resolution, λ is a constant coefficient associated to differential-non-differential transition, $f(\alpha)$ is the singularity spectrum of the order α , α is the singularity index and D_F is the fractal dimension of the “movement curves” [19,20].

There are many modes, and thus a varied selection of definitions of fractal dimensions; for example the fractal dimension in the sense of Kolmogorov, the fractal dimension in the sense of Hausdorff-Besikovitch etc. [19,20]. Selecting one of these definitions and operating it in the context of FeMnSiCrNi SMA,

the value of the fractal dimension must be constant and arbitrary for the entirety of the dynamical analysis. In the description of FeMnSiCrNi shape memory alloy it is regularly found that $D_F < 2$ for correlative processes and $D_F > 2$ for non-correlative processes etc.

In such a context, it is usually accepted the fact that stresses and strains at any point of any type of matter, are represented in a tensor form ($\hat{\sigma}_{ik}$ for stress tensor and $\hat{\varepsilon}_{ik}$ for the strain tensor, where $i, k = 1, 2, 3$) with the characteristic cubic equation for stress having the form:

$$\sigma^3 - I_1 \sigma^2 + I_2 \sigma - I_3 = 0 \tag{5}$$

and the corresponding characteristic cubic equation for strain having the form:

$$\varepsilon^3 - J_1 \varepsilon^2 + J_2 \varepsilon - J_3 = 0 \tag{6}$$

In relations (5) and (6), I_1, I_2 and I_3 are the invariants related to the stress tensor and J_1, J_2 and J_3 are the invariants related to the strain tensor. If it is supposed that stresses and strains are linked to the same material point, then from a physical point of view, it is necessary to describe a relationship between these stresses and strains.

Ideally speaking, the best course of action is to find the most general relationship which, when referring to the case of tensors, should be invariant when considering orthogonal groups. In such a context, said relationship should establish a correlation between I 's and J 's of equations (5) and (6).

As such, this general relationship can be written in the shape of a homographical transformation [35]:

$$\varepsilon_k = \frac{\alpha \sigma_k + \beta}{\gamma \sigma_k + \delta}, k = 1, 2, 3 \tag{7}$$

where σ_k and ε_k are the roots of equations (5) and (6) and α, β, γ and δ are real constants.

Thus, if the relation described by equation (7) is taken to represent a constitutive law, then the parameters α, β, γ and δ must be material parameters. Using equation (7) for a constitutive law, it is possible to describe the changes which occur in a material as a result of deformation using the material parameters α, β, γ and δ .

As such, a unique state of stress related to a certain state of strain, even as the structure of the material is changing, can be described. This is in line with the usual definition for the stresses and strains, which do not depend on any material. Consequently, only the constitutive law depends on the material.

Since every type of matter changes its structure when the deformation process takes place, said change can be reflected in the fact that the matter coefficients α, β, γ and δ , which make the constitutive law, vary with deformation. In these conditions, the matrix associated to the homographical transformation from (7) with the expression:

$$\hat{\alpha} = \begin{pmatrix} \alpha & \beta \\ \gamma & \delta \end{pmatrix} \tag{8}$$

becomes fundamental in the generation of the constitutive laws

for any type of matter – more precisely, in the differential geometry associated to this matrix.

In such a context, the FeMnSiCrNi SMA analysis in usual space, is reduced to the obtainment of a relation between the matrix ensemble \hat{a} and an ensemble of σ values through which σ' remains constant. Geometrically, this implies the searching of the ensemble of points $(\alpha, \beta, \gamma, \delta)$, which univocally corresponds to the values of the parameter σ . Using (7), the solution of the problem is reduced to a Riccati type gauge in the form:

$$d\sigma + \omega_1\sigma^2 + \omega_2\sigma + \omega_3 = 0 \tag{9}$$

where the following notations are used [36,37]:

$$\begin{aligned} \omega_1 &= \frac{\gamma d\alpha - \alpha d\gamma}{\Delta}, \\ \omega_2 &= \frac{\delta d\alpha - \alpha d\delta + \gamma d\beta - \beta d\gamma}{\Delta}, \\ \omega_3 &= \frac{\delta d\beta - \beta d\delta}{\Delta} \end{aligned} \tag{10}$$

with

$$\Delta = \alpha\delta - \gamma\beta \tag{11}$$

It is easy to verify the fact that the metric (ds^2):

$$ds^2 = \frac{(\delta d\alpha + \alpha d\delta - \gamma d\beta - \beta d\gamma)^2}{4\Delta^2} + \frac{d\alpha d\delta - d\beta d\gamma}{\Delta} \tag{12}$$

is in a direct relation with the discriminant from of the quadratic polynomial (9)

$$ds^2 = \frac{1}{4}(\omega_2^2 - 4\omega_1\omega_3) \tag{13}$$

The three differentiable l -forms from (10) completely define the coframe in every point of the absolute space. This coframe allows the translation of all geometric properties of the absolute space in the algebraic properties linked to (9) (36,37).

3.2.2. Stresses – strains behaviors of multifractal type

The simplest property refers to dynamics on the metric geodesics which can be correlated directly into statistical properties and from here the multi-fractalization through stochasticization (19,20). In this case, the l -forms $\omega_1, \omega_2, \omega_3$ are differentiable in the same parameter, *i.e.* τ :

$$\omega_1 = a_1 d\tau, \omega_2 = 2a_2 d\tau, \omega_3 = a_3 d\tau \tag{14}$$

Along this geodesic, (9) becomes a Riccati type equation (35-37):

$$\frac{d\sigma}{d\tau} = a_1\sigma^2 + 2a_2\sigma + a_3 \tag{15}$$

a_1, a_2, a_3 being constants that characterize certain geodesics from the family.

The equation (15) admits a direct integration, with three possible results:

$$\sigma(\tau) = -\frac{a_2}{a_1} + \frac{\sqrt{\Delta}}{a_1} \tan[\sqrt{\Delta}(\tau - \tau_0)] \text{ for } \Delta > 0 \tag{16}$$

$$\sigma(\tau) = \frac{a\tau + b}{c\tau + d} \text{ for } \Delta = 0$$

$$\sigma(\tau) = -\frac{a_2}{a_1} + \frac{\sqrt{\Delta}}{a_1} \coth[\sqrt{\Delta}(\tau - \tau_0)] \text{ for } \Delta < 0$$

Here, Δ and τ_0 are defined by the equations:

$$\Delta \equiv a_1 a_3 - a_2^2, a_2 = \sqrt{\Delta} \tan(\tau_0 \sqrt{\Delta}) \tag{17}$$

For the first case (16) and a, b, c, d are constants, not all of them arbitrary. One of the equations (16), depending on what the case may be, describes a deformation process at constant strain (a relaxation process).

The main procedure can be applied for strain (ε) analysis as well. Then,

$$\frac{d\varepsilon}{d\tau} = a_1\varepsilon^2 + 2a_2\varepsilon + a_3 \tag{18}$$

a_1, a_2, a_3 being constants that characterize certain geodesics from the family.

The equation (18) admits a direct integration, with three possible results:

$$\varepsilon(\tau) = -\frac{a_2}{a_1} + \frac{\sqrt{\Delta}}{a_1} \tan[\sqrt{\Delta}(\tau - \tau_0)] \text{ for } \Delta > 0 \tag{19}$$

$$\varepsilon(\tau) = \frac{a\tau + b}{c\tau + d} \text{ for } \Delta = 0$$

$$\varepsilon(\tau) = -\frac{a_2}{a_1} + \frac{\sqrt{\Delta}}{a_1} \coth[\sqrt{\Delta}(\tau - \tau_0)] \text{ for } \Delta < 0$$

Here, Δ and τ_0 (integration constant) are defined by the equations:

$$\Delta \equiv a_1 a_3 - a_2^2, a_2 = \sqrt{\Delta} \tan(\tau_0 \sqrt{\Delta}) \tag{20}$$

For the second case (19) and a, b, c, d are constants, not all of them arbitrary. One of the equations (18), depending on what the case may be, describes a deformation process at constant stress (a creep process).

Now, if a particular case is admitted:

$$a_1 = -f, 2a_2 = f, a_3 = 0 \tag{21}$$

the Riccati type equation (15) takes the form (*i.e.* a logistic type equation) [19, 20]:

$$\frac{d\sigma}{d\tau} = f\sigma(1 - \sigma) \tag{22}$$

Thus, the increase of σ is restricted by self-interaction effects of σ^2 (the “finite world/matrix” effect) (19,20). From (22) by integration, it results the solution:

$$\sigma = \frac{1}{1 - \left(1 - \frac{1}{\sigma_0}\right) \exp(-f\tau)} \quad (23)$$

where σ_0 is an integration constant.

A similar mathematical procedure applied to the Riccati type equation (18) implies the solution

$$\varepsilon = \frac{1}{1 - \left(1 - \frac{1}{\varepsilon_0}\right) \exp(-f\tau)} \quad (24)$$

where ε_0 is an integration constant.

In Fig. 5 the non-dimensional dependences creep strain – time for various temperatures are given, while the non-dimensional dependences creep strain rate-temperature for various forces is illustrated in Fig. 6. It results that the theoretical model is validated through the experimental date.

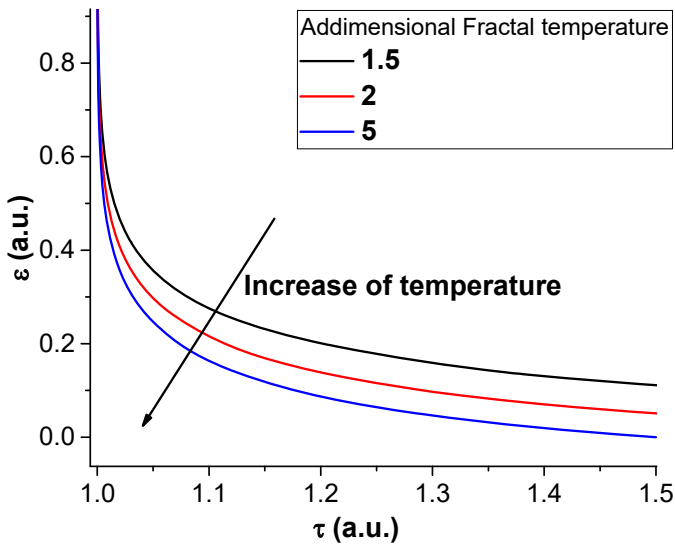


Fig. 5. Effects of fractal temperature on the variation of non-dimensional creep strain with time

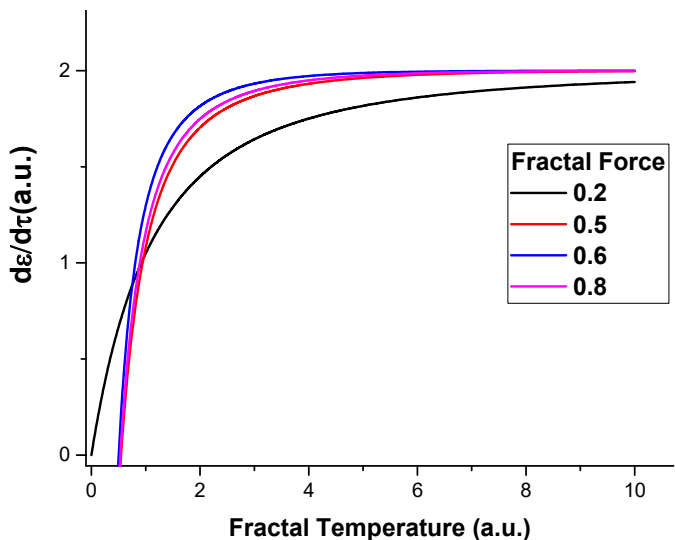


Fig. 6. Effects of fractal force on the variation of non-dimensional creep rate with temperature

4. Conclusions

The main conclusions of the present paper can be drawn at experimental and theoretical levels.

From an experimental point of view:

- A two-stage creep phenomenon was observed at Fe-18Mn-3Si-7Cr-4Ni (mass. %) SMA subjected to bending.
- Due to the very low amount of applied force (max. 9 N) and limited time (2000 s) the average value of bending deflection rate as a function of time and temperature varied between 4.77×10^{-6} and 9.35×10^{-6} $\mu\text{m}/(\text{s} \times ^\circ\text{C})$. These extremely small values demonstrate that secondary creep has been fully stabilized and its rate is almost insensitive to time, in the first 2000 s, even at temperatures as high as 300°C .

From a theoretical point of view, considering that the FeMnSi-CrNi SMA can be assimilated, both structurally and functionally, with a multifractal object, various behaviors of this shape memory alloy using the Multifractal Theory of Motion in the form of the multifractal hydrodynamic model have been analyzed. The following conclusions can be drawn:

- The expected form of the multifractal stress tensor has been given.
- The general relationship stresses- strains using the differential geometry was associated to the matrix of 2×2 type with real elements, the solution of the problem being reduced to Riccati type gauge.
- The dynamics on the metric geodesics could be directly correlated with stresses-strains constitutive laws which enabled to present creep phenomena in FeMnSiCrNi SMA, at various scale resolutions.
- The theoretical model was validated by means of experimental data.

REFERENCES

- [1] H. Otsuka, H. Yamada, T. Maruyama, S. Matsuda, M. Murakami, Effects of Alloying Additions on Fe-Mn-Si Shape Memory Alloys, *ISIJ Int.* **30**, 674-679 (1990).
- [2] Y. Moriya, H. Kimura, S. Ishizaki, S. Hashizume, S. Suzuki, H. Suzuki, T. Sampei, Properties of Fe-Cr-Ni-Mn-Si (-Co) shape memory alloys, *J. Phys. IV France* **01 C4**, 433-437 (1991).
- [3] Y.H. Wen, H. B Peng, D. Raabe, I. Gutierrez-Urrutia, J. Chen, Y.Y. Du, Large recovery strain in Fe-Mn-Si-based shape memory steels obtained by engineering annealing twin boundaries, *Nature Comm.* **5**, 4964 (2014). DOI: <https://doi.org/10.1038/ncomms5964>
- [4] H. Peng, G. Wang, S. Wang, J. Chen, I. Mac Laren, Y. Wen, Key criterion for achieving giant recovery strains in polycrystalline Fe-Mn-Si based shape memory alloys, *Mater. Sci. Eng. A.* **712**, 37-49 (2018). DOI: <https://doi.org/10.1016/j.msea.2017.11.071>
- [5] T. Sawaguchi, T. Maruyama, H. Otsuka, A. Kushibe, Y. Inoue, K. Tsuzaki, Design Concept and Applications of FeMnSi-Based Alloys from Shape-Memory to Seismic Response Control, *Mater. Trans.* **57** (3), 283-293 (2016). DOI: <https://doi.org/10.2320/matertrans.MB201510>

- [6] B. Pricop, A.U. Söyler, B. Özkal, L.G. Bujoreanu, Powder Metallurgy: An Alternative for FeMnSiCrNi Shape Memory Alloys Processing, *Front. Mater.* **7**, 247 (2020). DOI: <https://doi.org/10.3389/fmats.2020.00247>
- [7] B. Pricop, E. Mihalache, G. Stoian, F. Borza, B. Özkal, L.G. Bujoreanu, Thermo-mechanical effects caused by martensite formation in powder metallurgy FeMnSiCrNi shape memory alloys, *Powder Met.* **61** (4), 348-356 (2018). DOI: <https://doi.org/10.1080/00325899.2018.1492773>
- [8] B. Pricop, F. Borza, B. Ozkal, L.G. Bujoreanu, Influence of Thermal and Mechanical/Powder Processing on Microstructure and Dynamic Stiffness of Fe-Mn-Si-Cr-Ni Shape Memory Alloy, *Trans. Indian Inst. Met.* **74**, 1409-1418 (2021). DOI: <https://doi.org/10.1007/s12666-021-02215-8>
- [9] L. Ciuca, N.M. Lohan, B. Pricop, L.G. Bujoreanu, Study of tensile behaviour of Fe base shape memory alloys during mechanical cycling, *IOP Conf. Ser.: Mater. Sci. Eng.* **591**, 012009 (2019). DOI: <http://dx.doi.org/10.1088/1757-899X/591/1/012009>
- [10] Y. Bar-Yam, Dynamics of Complex Systems, The Advanced Book Program, Addison-Wesley, Reading, Massachusetts (1997).
- [11] M. Mitchell, Complexity: A Guided Tour, Oxford University Press, Oxford (2009).
- [12] R. Badii, Complexity: Hierarchical Structures and Scaling in Physics, Cambridge University Press (1997).
- [13] G.W. Flake, The Computational Beauty of Nature, MIT Press, Cambridge MA (1998).
- [14] D. Băceanu, K. Diethelm, E. Scalas, H. Trujillo, Fractional Calculus, Models and Numerical Methods, World Scientific, Singapore (2016).
- [15] M.D. Ortigueira, Fractional Calculus for Scientists and Engineers, Springer (2011).
- [16] L. Nottale, Scale Relativity and Fractal Space-Time: A New Approach to Unifying Relativity and Quantum Mechanics, Imperial College Press, London (2011).
- [17] I. Merches, M. Agop, Differentiability and fractality in dynamics of physical systems, World Scientific, New Jersey (2016).
- [18] M. Agop, V.P. Paun, On the new perspectives of the fractal theory. Fundamentals and applications, Romanian Academy publishing house, Bucharest (2017).
- [19] E.A. Jackson, Perspective of nonlinear Dynamics, volume 2, Cambridge University Press, Cambridge (1991).
- [20] C.P. Cristescu, Nonlinear dynamics and chaos. Theoretical fundamentals and applications, Romanian Academy Publishing House, Bucharest (2008).
- [21] M. Agop, P.E. Nica, S. Gurlui, C. Focsa, V.P. Paun, M. Colotin, Implications of an extended fractal hydrodynamic model, *The European Physical Journal D.* **56**, 405-419 (2010).
- [22] M. Agop, V.P. Paun, A. Harabagiu, El Naschie's $\varepsilon(\infty)$ theory and effects of nanoparticle clustering on the heat transport in nanofluids, *Chaos Solitons & Fractals* **37** (5), 1269-1278 (2008).
- [23] M. Agop, P.E. Nica, P.D. Ioannou, A. Antici, V.P. Paun, Fractal model of the atom and some properties of the matter through an extended model of scale relativity, *The European Physical Journal D.* **49** (2), 239-248 (2008).
- [24] M. Agop, C. Murgulet, El Naschie's $\varepsilon(\infty)$ space-time and scale relativity theory in the topological dimension $D = 4$, *Chaos, Solitons & Fractals* **32** (3), 1231-1240 (2007).
- [25] S. Gurlui, M. Agop, M. Strat, G. Strat, S. Bacaita, A. Cerepaniuc, Some experimental and theoretical results on the anodic patterns in plasma discharge, *Physics of plasmas* **13** (6), 063503-06350310 (2006).
- [26] I. Gottlieb, M. Agop, M. Jarcau, El Naschie's Cantorian space-time and general relativity by means of Barbilian's group. A Cantorian fractal axiomatic model of space-time, *Chaos, Solitons & Fractals* **19** (4), 705-730 (2004).
- [27] C. Nejneru, A. Nicuta, B. Constantin, L.R. Manea, M. Teodorescu, M. Agop, Dynamics Control of the Complex Systems via Nondifferentiability, *J. App. Math.* **2013** (SI19), 1-12 (2013).
- [28] I. Casian-Botez, M. Agop, P. Nica, V.P. Paun, G.V. Muncelleanu, Conductive and Convective Types Behaviors at Nano-Time Scales, *J. Comput. Theor. Nanosci.* **7** (11), 2271-2280 (2010).
- [29] O. Niclescu, D.G. Dimitriu, V.P. Paun, P.D. Matasaru, D. Scurtu, M. Agop, Experimental and theoretical investigations of a plasma fireball dynamics, *Physics of Plasmas* **17** (04), 2305-042305 (2010).
- [30] M. Colotin, G.O. Pompilian, P. Nica, S. Gurlui, V. Paun, M. Agop, Fractal transport phenomena through the Scale Relativity Model, *Acta Phys. Polon. A* **116**, 157-164 (2009).
- [31] M. Agop, P. Nica, M. Girtu, On the vacuum status in Weyl-Dirac theory, *General Relativity and Gravitation* **40** (1), 35-55 (2007).
- [32] I. Gottlieb, M. Agop, G. Ciobanu, A. Stroe, El Naschie's $\varepsilon(\infty)$ space-time, hydrodynamic model of scale relativity theory, *Chaos, Solitons & Fractals* **34** (5), 1704-1723 (2007).
- [33] I. Gottlieb, M. Agop, G. Ciobanu, A. Stroe, El Naschie's $\varepsilon(\infty)$ space-time and new results in scale relativity theories, *Chaos Solitons & Fractals* **30** (2), 380-398 (2006).
- [34] C. Leinenbach, W.J. Lee, A. Lis, A. Arabi-Hashemi, C. Cayron, B. Weber, Creep and stress relaxation of a FeMnSi-based shape memory alloy at low temperatures, *Mat. Sci. Eng. A* **677**, 106-115 (2016). DOI: <https://doi.org/10.1016/j.msea.2016.09.042>
- [35] W.S. Burnside, A.W. Panton, The theory of Equations, Dova Publishing (1960).
- [36] N. Mazilu, M. Agop, Skyrmions: A Great Finishing Touch to Classical Newtonian Philosophy, *Wold Philosophy Series, Nova New-York* (2012).
- [37] N. Mazilu, M. Agop, I. Merches, The Mathematical Principles of Scale Relativity Physics. The concept of Interpretation, CRC Press Taylor, Francis Group (2020).